Dispersive FDTD Analysis of Induced Electric Field in Human Models Due to Electrostatic Discharge

Akimasa Hirata[1], Toshiyuki Nagai, Teruyoshi Koyama, Junya Hattori, Kwok Hung Chan and Robert Kavet

1: Nagoya Institute of Technology, Department of Computer Science and Engineering, Japan

2: Electric Power Research Institute, Palo Alto, California, USA

Corresponding Author: Akimasa Hirata

Address: Nagoya Institute of Technology, Gokiso-cho, Showa-ku, Nagoya 466-8555, Japan

Tel&Fax: +81-52-735-7916

E-mail: ahirata@nitech.ac.jp

Abstract

Contact currents flow from/into a charged human body when touching a grounded conductive object. An electrostatic discharge (ESD) or spark may occur just before contact or upon release. The current may stimulate muscles and peripheral nerves. In order to clarify the difference in the induced electric field between different sized human models, the *in-situ* electric fields were computed in anatomically-based models of adults and a child for a contact current in a human body following electrostatic discharge. A dispersive finite-difference time-domain method was used, in which biological tissue is assumed to obey a 4-pole Debye model. From our computational results, the first peak of the discharge current was almost identical across adult and child models. The decay of the induced current in the child was also faster due mainly to its smaller body capacitance compared to the adult models. The induced electric fields in the forefingers were comparable across different models. However, the electric field induced in the arm of the child model was found to be greater than that in the adult models primarily because of its smaller cross-sectional area. The tendency for greater doses in the child has also been reported for power frequency sinusoidal contact current exposures as reported by other investigators.

1. Introduction

Extremely-low-frequency electric fields couple directly to people and animals, inducing currents within the body's tissues. Electric fields also produce indirect interactions (1) through surface charge effects, such as hair vibration; (2) by producing a continuous contact current between a person and an object the person touches (contact current), with current flow determined by the respective impedances to ground of the person and object; and (3) by producing an electrostatic discharge (ESD) (also known as spark discharge) between the person and object either prior to contact with or upon release of the object. For frequency components <100 kHz, the main effect of ESD is electrostimulation, with heating effects dominating at higher frequencies (IEEE 2002, ICNIRP 2010). The amount of charge transferred during an ESD depends on the electric field magnitude, the relative sizes of the person and the object contacted, and the complex impedances of each to ground.

Several studies have reported *in situ* dose from ESD exposure in anatomical models of human adults. Amoruso *et al* (2000) calculated the induced currents in a human body based on a circuit model consisting of lumped circuit parameters, and then evaluated currents induced in several body parts. They did not take model morphology into account, and electric fields induced in specific neural tissues could not be calculated. Okoniewska *et al* (2004) used finite difference time domain (FDTD) method to calculate electric fields and specific absorption (SA) in an anatomically correct human model exposed to ESD. They injected into the forefinger an ESD waveform specified in the International Electrotechnical Commission (IEC) standard 61000-4.2 for immunity testing. Two issues with this analysis are: first, the IEC current waveform is reported to differ from an ESD to which people are typically exposed (Kagawa *et al* 2010), and second, the tissue model was non-dispersive. To address the latter issue, the same laboratory used a frequency domain approach to analyze dose to tissue from the IEC pulse (Dawson *et al* 2004a). They also compared electric fields in tissue resulting from the pulse to the electrostimulation thresholds predicted by the tissue-specific strength-duration curves (Dawson *et al* 2004b). In our laboratory, we computed transient contact current and *in-situ* electric fields in a charged human represented by a Japanese adult male model by taking into account dispersive characteristics of exposed to a realistic ESD (Nagai *et al* 2010).

Dosimetric analyses of ESD to date, however, have not examined the differences between adults and children with respect to induced quantities and thresholds of electrostimulation. We do know that children's sensory thresholds for continuous contact current are roughly one-half their values in adults (IEEE Working Group on Electrostatic and Electromagnetic Effects 1978, Chatterjee *et al* 1986). Strength duration curves have been derived largely from *in-vitro* studies (e.g., Rogers *et al* 2004), with a limited amount of data published on temporal characteristics of ESD in human subjects (Reilly and Larkin 1983, Nagai *et al* 2009), and virtually none on

children.

In this paper, we present a novel study on characterizing the ESD dosimetry in skin and subcutaneous fat, which are served as a surrogate for peripheral nerve, in human bodies. We apply the FDTD method to compute transient contact currents and the resultant *in-situ* electric fields from charged human models including a child model. We then discuss the primary factors affecting the ESD waveforms as they relate to the threshold of electrostimulation. We considered the dosimetry in the skin and subcutaneous fat (as surrogates for peripheral nerve), brain, and muscle, as Dawson *et al* (2004a) did, because these are the key tissue sites relevant to the setting of contact current (and electric and magnetic field) exposure limits (IEEE 2002, ICNIRP 2010).

2. Model and Methods

2.1. Human Body Models

A full description of the Japanese adult male and female voxel models, TARO and HANAKO is given in Nagaoka *et al* (2004). The average height and weight of Japanese who are 18 to 30 years old are 1.714 m and 63.3 kg for males, and 1.591 m and 52.6 kg for females (NIBH 1996). Volunteers were selected whose dimensions were close to the average values. The male volunteer was 22 years old, 1.728 m tall, and weighed 65.0 kg; the female volunteer was 22 years old, 1.6 m tall, and weighed 53.0 kg. Based on magnetic resonance images, the voxels were scaled to 2 mm cubes and segmented to define 51 discrete tissues and organs. The 3-year-old child phantom was developed by applying a free-form deformation algorithm to TARO (Nagaoka *et al* 2008). In the deformation, 66 body dimensions were taken into account. The resolution of the child model was kept at 2 mm. The height and weight of the 3-year-old child model were 0.90 m and 13 kg, respectively. Bone marrow was manually added only in the arm to investigate the induced electric field. As indicated below, the arm and fingers of the models are bent manually to realistically simulate human contact with a metallic object.

2.2. Computational Methods

Modeling with the dispersive characteristics of human tissues becomes necessary here because transient current from a charged human contains ultra-wide frequency components (Amoruso *et al* 2000, Okoniewska *et al* 2004). There are several studies in which dosimetry has taken into account the dispersive characteristics of the human body assuming that the biological tissue obeys one-pole Debye medium (e.g., Simicevic 2005). However, the bandwidth considered therein was insufficient to cover the spectra of ESD-induced currents and electric fields, which may include DC to 10 GHz or higher. To account the frequency-dependent

properties of tissue over ultra wideband, we assumed that human tissues obey the dispersion properties of a *four-pole* Debye medium, which can be expressed as (Hirata *et al* 2010b)

$$\varepsilon_r(\omega) = \varepsilon_\infty + \sum_{p=1}^{4} \frac{\Delta\varepsilon_p}{1 + j\omega\tau_p} + \frac{\sigma_0}{j\omega\varepsilon_0} \quad (1)$$

where $\varepsilon_r(\omega)$ is the complex relative permittivity; ε_∞, the relative permittivity at infinite frequency; σ_0, the DC conductivity; $\Delta\varepsilon_p$, the change in the p-pole relative permittivity; τ_p, the p-pole relaxation time; and ε_0, the free-space permittivity. The parameters in (1) were determined by the least-squares method in comparison with a 4-Cole-Cole model from 10 kHz to 10 GHz (Gabriel *et al* 1996), and have been reported previously (Hirata *et al* 2010b). Even though we chose 10 kHz as the lower frequency bound, our computational modelling was shown to be reasonable for much lower frequencies (Hirata *et al* 2010b). This is because the electrical conductivity of tissue is almost constant at frequencies below 10 kHz, in addition to the fact that, below the MHz range, the conduction current is dominant compared to the displacement current (Dawson *et al* 2004a). The electrical conductivities of the child were assumed to be the same as those of the adults. This assumption is supported by the facts that 1) the dielectric properties of tissues are mainly determined by their water content and 2) the water contents of a 3-year-old and an adult are not so different (Wang *et al* 2006).

2.3. Exposure Scenario

We model a scenario in which a charged human contacts ground through a hand-held piece of metal. The contact with the piece of metal makes the measurement more reproducible, since the fingertip contact without hand-held piece of metal produced multiple-shot discharge current with a gently rising time and low amplitudes (Kagawa *et al* 2010). Note that the piece of metal would have a larger effective contact area than that without the piece of metal and hence induced electric field is lower than that of actual phenomena.

Figure 1 shows the FDTD model used for analyzing contact currents and *in-situ* electric fields. The side length of the FDTD cell was 2 mm, to coincide with the human model resolution. The human model was placed at a distance of *d* above the ground plane. For the metal bar, we used a metallic tip electrode with a curvature of 4 mm (8 mm in diameter), which is employed as the current injection electrode of an ESD gun. An aluminium plate (1 m × 2 m) was used as a ground and was positioned vertically on a square aluminium plate with a side of 1 m. ESD exposure to the human body was simulated with applying a step voltage across a one-cell gap between the hand-held metal piece and the vertical ground plate.

2.4. Threshold for Electrostimulation

Nerves and muscle cells can be excited by electrical stimulation. The threshold of nerve and muscle excitation is described in the strength-duration curve (Reilly 2003):

$$E_T = E_0 \left[1 - \exp(-t / \tau_e)\right]^{-1} \quad (2)$$

where E_T denotes the threshold electric field; E_0, the minimum (rheobase) threshold; τ_e, the strength-duration time constant; and t, the pulse duration. For the peripheral nerve, values of E_0 and τ_e were reported to be 6.15 V/m and 0.149 ms (Reilly 2003), and 3.6 V/m and 0.36 ms (Dawson *et al* 2004b), respectively. τ_e was reported by Nyenhuis *et al* (2001) to be 0.1 ms, with a rheobase of 2.2 V/m based on computational dosimetry. Recently, the time constant for electric and magnetic stimulation has been reported to be different (Recoskie *et al* 2009) and the possible reasons have also been discussed by Reilly (2010). However, conclusion has not yet been obtained at this moment. Thus, we included the following range in this paper: E_0 varied from 2 V/m to 6.15 V/m, and τ_e, from 0.1 to 0.36 ms. To date, no study has used this range of values to characterize effects from a charged human body.

3. Result

3.1. Discharge Current

Figure 2 shows computed waveforms of the contact currents through a hand-held piece of metal from the human models with a charge voltage (V_C) of 1 kV. For comparison the result from a human subject (1.77 m, 60 kg) exposed under the same conditions is included in Figure 2(a). The measured and computed rise times of the waveform are in good agreement with each other (Fig. 2(a)). As also seen from Fig. 2 (a), the peak measured current amplitude is 33% smaller than the computed peak. The field amplitude in the 3-year-old child model decays with a time constant of 43 ns compared to slower decay in the adult models with a time constant of 72.1 ns for the female and 89.6 ns for the male.

3.2. *In-Situ* Electric Field

Induced electric fields in the arm of the adult and child models are compared in Fig. 3. From Fig. 3(a), the maximum electric fields in the fat of the models appeared around the conductor (y = 42 mm for a 3-year-old child, and y = 32 mm for adults). From Fig. 3(b), the layer-averaged value of induced field (all tissue) becomes maximal around the wrist, as well as at the conductor. Except around the conductor, the *in-situ* electric field of the 3-year-old child model was larger than those of the adult models. As shown in Table 1, the maximum electric fields induced in the adult male, adult female and child models' bone marrow were 0.75 kV/m, 0.82 kV/m and 1.8 kV/m, respectively and for the brain were 0.021 kV/m, 0.023 kV/m and 0.052 kV/m, respectively. The greatest maxima were in the skin, muscle and fat.

3.3. Comparison between *In-Situ* Electric Field and S-D Curves

When the stimulus duration, $t << \tau_e$, the threshold for electrostimulation in terms of charge remains constant, for all practical purposes, with a value in direct proportion to $E_0 \times \tau_e$ (Reilly 2003). Based on the published estimates of E_0 and τ_e for peripheral nerve, brain neuron (white matter) and cardiac tissue, we compared the time integral of the *in-situ* electric field to $E_0 \times \tau_e$ to evaluate exceedance of electrostimulation thresholds for each tissue across models. Table 2 indicates that brain and heart remain well below threshold in all three models. For skin and fat, representing peripheral nerve, the male model's threshold are exceeded by a fair margin, whereas the female and child integrals fall into the gray range, suggesting that electrostimulation threshold would be exceeded for all estimates of E_0 and τ_e with a marginally greater voltage stimulus (about 60%). The larger time integral of the *in-situ* electric fields in the brain and heart of the child model compared to the adult models is caused by the distances from the finger to the respective tissues.

4. Discussion

4.1. Discharge Current

We used a step voltage across a one-cell gap between the hand-held metal piece and the vertical ground plate (Sec 2.3). Because of our source modelling, the peak measured current amplitude is 33% smaller than the computed peak (Fig. 2(a)), providing the conservative induced fields. However as discussed in Nagai *et al* (2009), the difference between peak measured and computed current amplitude decreases to a few percent when improved source modelling is used. However, in that modelling, the measured time course of voltage is required, and was not possible in the child model's computation due to the absence of measurement data for ethical reasons. Thus, we applied the step voltage for all the models considered herein.

The contact current from an ESD into either of our models or a human subject rises steeply with no differences in rise time among models or between the models and human subjects. The decay was comparatively much faster, with a smaller time constant in the child model compared to the adult models. The initial current time course is due to the discharge from the stray capacitance between the piece of metal and the ground, with no differences among models expected. The remainder of the current plot varies across models because of their morphological differences (Kagawa *et al* 2010). These differences translate to calculated body capacitances of 105 pF, 100 pF and 56 pF for the adult male, adult female and 3-year-old child, respectively (see Appendix A). The time constants of the current decay curve, τ, were estimated from the data for Fig. 2 (b) as 89.6 ns, 72.1 ns and 43.0 ns for the phantoms of the adult male, adult female and 3-year-old child models, respectively. Their body resistances were then, respectively,

estimated (τ/C) as 853 Ω, 721 Ω and 768 Ω, respectively. Thus, the difference in the time constant is mainly attributable to the differences in body capacitance.

4.2. *In-situ* Electric Field and Threshold of Electrostimulation

The maximum value of the *in-situ* field is dependent on the anatomical composition of the hand and its relationship with the piece of metal it holds. Note that the finger does not contain muscle. The maximum induced electric fields in the three models were all comparable, as the first peaks of the waveform of the discharge current were almost identical, as shown in Fig. 2 (a), and the contact areas of fingers with metal piece were comparable among models. Different amounts of total charge accumulated in the body are caused by the differences in human body capacitance, as covered in Sec. 4. 1.

The layer-averaged values were primarily affected by the cross-sectional area of the arm, with the maximum value seen in the wrist for each model (Figure 3(b)). The cross sectional areas of the wrist for the adult male and adult female and 3-year-old model were 25.5 cm^2, 19.8 cm^2 and 6.2 cm^2, respectively, and the layer-averaged *in-situ* fields were, respectively, 4.5 kV/m, 7.2 kV/m and 11.2 kV/m. Thus, wrist cross-section and its layer-averaged electric field are approximately inversely related to each other, which has also been suggested for a sinusoidal contact current (Sweeney 1993). The perception threshold in the wrist of the charged human body may be determined by the balance of accumulated charge and cross sectional-area.

The present study reports dosimetry relevant to electrostimulation caused by ESD. However, we point out two main uncertainty/variability factors. The first is the singular behaviour of the electromagnetic field, especially for the low-frequency component, caused by using the model with staircasing artefact (Dawson *et al* 2001). However, this factor is at most several percent for contact current, unlike external field exposure (Hirata *et al* 2011). The second uncertainty concerns the difference in the charge thresholds of electrostimulation, which is attributable to experimental conditions such as electrode size (Reilly and Larkin 1983). The reported values of the minimum charge threshold for perception of short duration pulses vary from 0.12 μC (Rollman 1974) to 0.88 μC (Heckmann 1972). In our previous study (Nagai *et al* 2009), for which the scenario was identical to the scenario considered herein, the threshold was 0.26-0.40 μC, corresponding to the computationally estimated charged voltage of 2.5–3.9 kV for the adult male, 2.6-4.0 kV for the adult female, and 4.0-7.1 kV for the child. By linearly scaling the data presented in Table 2 to these voltages, the computed product of E_0 and τ_e (which represents the charge criteria) in this paper would be readily exceeded. One of the primary reasons why the computed results are larger than the expected threshold would be the masking effect of the piece of metal (Reilly and Larkin 1983) and the difference in contact area. For the latter factor, it is

difficult to discuss in the straightforward manner as the current density in the contact area is non-uniform.

As shown in Table 2, the time integral of induced electric field in the brain and heart were much smaller than the threshold derived from the strength-duration curve by a factor of 100 in the adult and 40 in the child model. Thus, stimulation may not occur in the body parts except for the contacting limb and the lower extremities as reported by Dawson *et al* (2004a, 2004b).

Summary

In order to understand the effect of body morphology on ESD dosimetry, we computed the *in-situ* electric fields in anatomically-based charged models of two adults and a child following a step discharge into the ground. A dispersive finite-difference time-domain method was used, in which biological tissue is assumed to obey a 4-pole Debye model. From our computational results, the first peak of the discharge current was the same across all three models, and moreover, the computed waveforms were in fair agreement with measurements conducted on human subjects. The temporal characteristic of the induced electric field in the child differed from that observed in the adults, which is primarily attributable to the differences in body capacitance. The induced electric fields were generally comparable for different models at the same charged voltage. However, in the arm, the *in-situ* electric field of the child was greater than that of the adult models primarily because of its smaller cross-sectional area. The *in-situ* electric field in the central nervous system was much smaller than the threshold. By comparing the computed *in-situ* electric field with the strength-duration curve, we determined whether the perception threshold was exceeded by computing the accumulated charge or the capacitance of the model for the same charged voltage applied to all models.

Appendix. A. Human Body Capacitance

For the scenario shown in Fig. 1, the human body model was charged to a voltage of V. The quasi-static FDTD method for contact current was used (Hirata *et al* 2010a) to calculate the total charge accumulated on the model surface. In addition, the surface charge of each cell of air adjacent to the model surface was computed using Gauss's law:

$$q_n = \int_S \boldsymbol{D}_n \cdot d\boldsymbol{S} \tag{A.1}$$

Then, the total charge accumulated on the model surface was computed as

$$Q = \sum_{n=1}^{N} q_n \,. \tag{A.2}$$

Finally, human body capacitance C was derived from the quotient Q/V.

Figure A1 illustrates two scenarios for charging the human body models. In the first scenario, the human body stands above a perfect ground at a distance of d. The second is the ESD scenario with the hand-held piece of metal described in Sec. II. Fig. A2 shows the human body capacitance for different body-ground distances. In order to verify our FDTD results, the computation with the surface charge (SC) approach is also shown. We saw good agreement between the quasi-static FDTD method and the body surface charge method (Fig. A2). Fair agreement was also obtained between measurement data from Fujiwara *et al* (1998) and our computational results (Fig. A2). .

The cumulative charge of the male adult model was shown in Fig. A3. For the model standing in free space (upright) the charge was mainly accumulated in the feet (Fig.A3(a)). For the scenario shown in Fig. 1, the body capacitance was larger than that for the model standing in free space for both adult and the child model (Table A1). This larger capacitance in the model with the arm bent was due to the capacitance between the perfect conductor and the arm.

References

Amoruso V, Helali M and Lattarulo F, 2000 An improved model of man for ESD applications. *J. Electrostat.* **49** 225–44.

Chatterjee I, Wu D, Gandhi O P 1986 Human body impedance and threshold currents for perception and pain for contact hazard analysis in the VLF-MF band *IEEE Trans Biomed Eng*, **33** 486-94

Dawson T W, Potter M and Stuchly M A 2001 Evaluation of modeling accuracy of power frequency field interactions with the human body. *ACES Journal* **16**, 162–72.

Dawson T W, Stuchly M A and Kavet R 2004a Electric fields in the human body due to electrostatic discharge. *IEEE Trans. Biomed. Eng.* **51** 1460–8.

Dawson T W, Stuchly M A and Kavet R 2004b Evaluation of interactions of electric fields due to electrostatic discharge with human tissue. *IEEE Trans. Biomed. Eng.* **51** 2194–8.

Fujiwara O and Ikawa T1998 Numerical calculation of human-body capacitance by surface charge method. *IEICE Trans.* **J84-B** 1841–7.

Gabriel S, Lau R W and Gabriel C 1996. The dielectric properties of biological tissues: 3. Parametric models for the dielectric spectrum of tissues. *Phys. Med. Biol.* **41** 2271–93.

Heckmann J R 1972 Excitability curve: A new technique for assessing human peripheral nerve excitability in vivo. Neurology **22** 224–30.

Hirata A, Takano Y and Nagai N 2010a Quasi-static FDTD method for dosimetry in human due to contact current. *IEICE Trans. Electron.* **E93-C** 60–5.

Hirata A, Nagai T, Koyama T and Fujiwara O 2010b Propagation of ESD-induced ultra-wideband electromagnetic pulse in the human body. *IEEE Antennas & Wireless Propagat. Lett.* **9** 1245–7.

Hirata A, Hattori J, Takano Y, Fujiwara O and Suzuki Y 2011 Computational uncertainty of induced electric field in human body due to contact current. *Proc. Int'l Congress of European Bioelectromagnet. Assoc.*

IEEE Working Group on Electrostatic and Electromagnetic Effects 1978 Electric and magnetic field coupling from high voltage AC power transmission lines –classification of short-term effects on people *IEEE Trans Power Apparatus Sys.* **97** 2243-52

International Commission on Non-Ionizing Radiation Protection (ICNIRP) 1998 Guidelines for limiting exposure to time-varying electric, magnetic, and electromagnetic fields (up to 300 GHz). *Health Phys.* **74** 494–522.

International Electrotechnical Commission (IEC). 2001 Electromagnetic Compatibility (EMC) - Part 4-2: Testing and measurement techniques - Electrostatic discharge immunity test IEC61000-4-2 Edition 1.2 2001–04.

Institute of Electrical and Electronics Engineers (IEEE) 2002 IEEE Standard for Safety Levels with Respect to Human Exposure to Electromagnetic Fields, 0–3 kHz. IEEE Std C95.6-2002.

Kagawa Y, Taka Y, and Fujiwara O 2010 Characteristic measurement of spark transients due to finger touch. *J. Electrostatics* **68** 1–4.

Okoniewska, E, Stuchly, M A and Okoniewski, M 2004 Interactions of electrostatic discharge with the human body. *IEEE Trans. Microwave Theory Tech.* **52** 2030–39.

Rogers W R, Merritt J H, Comeaux Jr. J A, Kuhnel C T, Moreland D F, Teltschik D G, Lucas J H and Murphy M R 2004 Strength-duration curve for an electrically excitable tissue extended down to near 1 nanosecond. *IEEE Trans. Plasma Sci.* **32** 1587–99.

Nagai T, Hirata A, and Fujiwara O, 2009 Electric field and its stimulation threshold in a hand induced by conductor contact of charged human. *Proc. IEICE General Conf.* B-4-27.

Nagai T and Hirata A, 2010 In-situ electric fields causing electro-stimulation from conductor contact of charged human, Radiation Protection Dosimetry, **140** 351–6.

Nagaoka, T, Watanabe, S, Sakurai, K, Kunieda, E, Watanabe, S, Taki, M and Yamanaka, Y 2004 Development of realistic high-resolution whole-body voxel models of Japanese adult males and females of average height and weight, and application of models to radio-frequency electromagnetic-field dosimetry. *Phys. Med. Biol.* **49** 1–15.

Nagaoka T, Kunieda E and Watanabe S 2008 Proportion-corrected scaled voxel models for Japanese children and their application to the numerical dosimetry of specific absorption rate for frequencies from 30 MHz to 3 GHz *Phys. Med. Biol.* **53** 6695–711.

NIBH 1996 Human Body Dimensions Data for Ergonomic Design (Tokyo: Research Institute of Human Engineering for Quality Life).

Nyenhuis J A, Bourland J D, Kildishev A V and Schaefer D J 2001 Health effects and safety of intense gradient fields. In: Shellock FG, ed. Magnetic resonance procedures: Health effects and safety. New York: CRC Press; 31–53.

Recoskie B J, Scholl T J, Chronik B A 2009 The discrepancy between human peripheral nerve chronaxie times as measured during magnetic and electric field stimuli: the relevance to MRI gradient coil safety *Phys. Med. Biol.* 54 5965-79

Reilly J P 2003 Mechanisms of electrostimulation: application to electromagnetic field exposure standards at frequencies below 100 kHz. in The International EMF Dosimetry Handbook, Chadwick, P. and Gabriel, C. eds. Online: http://www.emfdosimetry.org.

Reilly J P and Larkin W D 1983 Electrocutaneous stimulation with high voltage capacitive discharges. IEEE Trans. Biomed. Eng. **30** 631–41.

Reilly J P, Diamant, A M and Comeaux, J 2009 Dosimetry considerations for electrical stun devices. *Phys. Med. Biol.* **54** 1319–35.

Reilly J P 2010 Comments on the discrepancy between human peripheral nerve chronaxie times as measured with magnetic and electric field stimuli: the relevance of MRI gradient coil safety. *Phys. Med. Biol.* **55** L5 – L8.

Rollman G B 1974 Electrocutaneous stimulation. in Conference on Cutaneous Communication Systems and Devices, Geldard, F. A. ed. (Austin, TX: Psychonomic Soc.) 38–51.

Simicevic N 2005 Three-dimensional FDTD simulation of biomaterial exposure to electromagnetic nanopulses. *Phys. Med. Biol.* **50** 5041–53.

Sweeney J D 1993 A theoretical analysis of the "let-go" phenomenon *IEEE Trans. Biomed. Eng.* **40** 1335–38.

Wang J, Fujiwara O and Watanabe S 2006 Approximation of aging effect on dielectric tissue properties for SAR assessment of mobile telephones. *IEEE Trans. Microwave Theory & Tech.* **48** 408–13.

World Health Organization (WHO). Environmental Health Criteria 238 Extremely Low Frequency Fields (2007).

Figure and Table Captions

Figure 1. FDTD model used for the analyses of contact currents and *in-situ* electric fields.

Figure 2. Computed waveforms of contact currents from charged human body models. Measured value by Kagawa *et al* (2010) is also plotted for comparison. (a) Linear plot for 0 to 10 ns and (b) log plot for 10 to 200 ns.

Figure 3. (a) Cell-maximum *in-situ* electric fields of fat and (b) layer-averaged in-situ electric field (all tissue). The charge voltage was 1.0 kV.

Table 1. Spatiotemporal maximum of in-situ electric field [kV/m] in tissues of adult and child models.

Table 2. Time integral of electric field (mV-s/m) in tissue compared to constant charge criterion. The skin and fat serve as a surrogate for peripheral nerve

Figure A1. FDTD model for computing the human body capacitance: (a) standing in free space and (b) realistic scenario for contact current.

Figure A2. Human body capacitance computed with the FDTD and surface charge (SC) methods for different human-ground distances. Measured values by Fujiwara and Ikawa (1998) are also plotted for comparison.

Figure A3. (a) Charge distribution on the human body surface and (b) cumulative capacitance of the human body.

Table A1. Human body capacitances for different human body models.

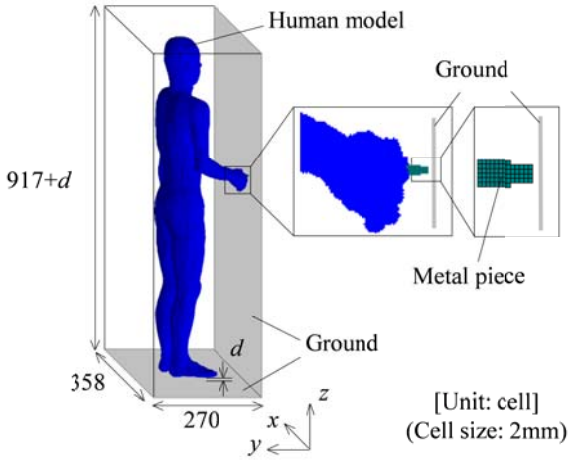
Human model
Ground
917+d
Metal piece
Ground
d
358
270
x
z
y
[Unit: cell]
(Cell size: 2mm)

Fig. 1

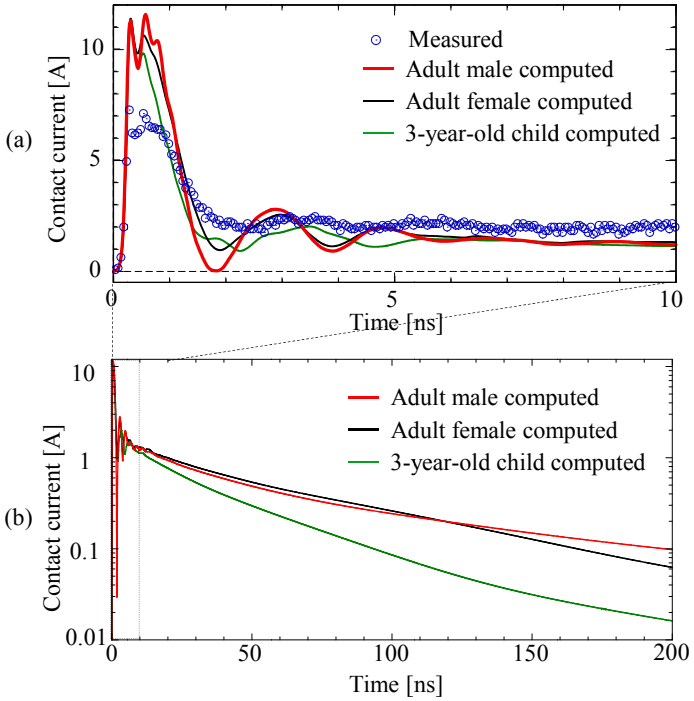
(a)
Contact current [A]
10
5
0
0
5
10
Time [ns]
Measured
Adult male computed
Adult female computed
3-year-old child computed
(b)
Contact current [A]
10
1
0.1
0.01
0
50
100
150
200
Time [ns]
Adult male computed
Adult female computed
3-year-old child computed

Fig. 2

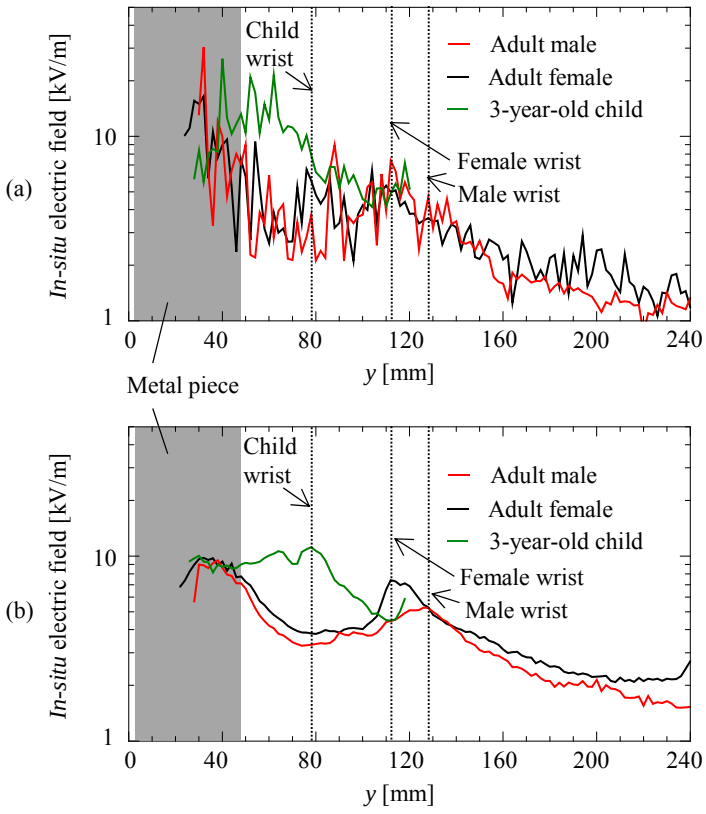
(a)
In-situ electric field [kV/m]
10
1
0
40
80
120
160
200
240
y [mm]
Child wrist
Adult male
Adult female
3-year-old child
Female wrist
Male wrist
Metal piece
(b)
In-situ electric field [kV/m]
10
1
0
40
80
120
160
200
240
y [mm]
Child wrist
Adult male
Adult female
3-year-old child
Female wrist
Male wrist

Fig. 3

Table 1.

Tissue	Male	Female	Child
Skin	70.1	47.2	56.3
Muscle	55.4	46.5	54.1
Fat	99.5	45.9	23.5
Bone Marrow	0.75	0.82	1.8
Brain	0.2	0.3	0.5
Heart	0.3	0.4	1.0
Blood	11.7	4.4	10.2

Table 2.

Tissue	Male	Female	Child	Criteria
Skin	3.71	1.81	1.46	~0.22-2.2
Fat	5.19	1.52	1.40	
Brain	8.69×10^{-3}	5.73×10^{-3}	2.13×10^{-2}	1.83
Heart	0.3	0.4	1.0	36

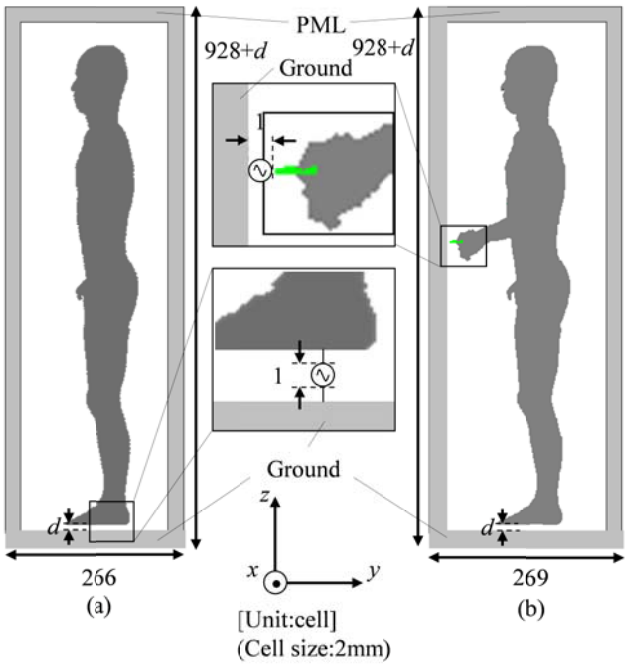
PML
928+d
928+d
Ground
1
1
Ground
d
d
z
x
y
266
(a)
269
(b)
[Unit:cell]
(Cell size:2mm)

Fig. A1

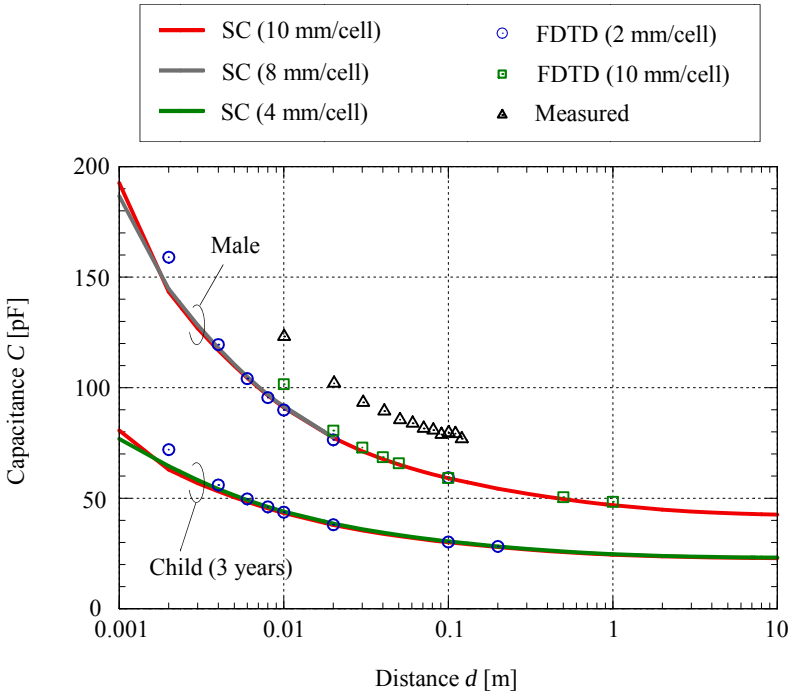
SC (10 mm/cell)
SC (8 mm/cell)
SC (4 mm/cell)
FDTD (2 mm/cell)
FDTD (10 mm/cell)
Measured
Male
Child (3 years)
Capacitance C [pF]
Distance d [m]
200
150
100
50
0
0.001
0.01
0.1
1
10

Fig. A2

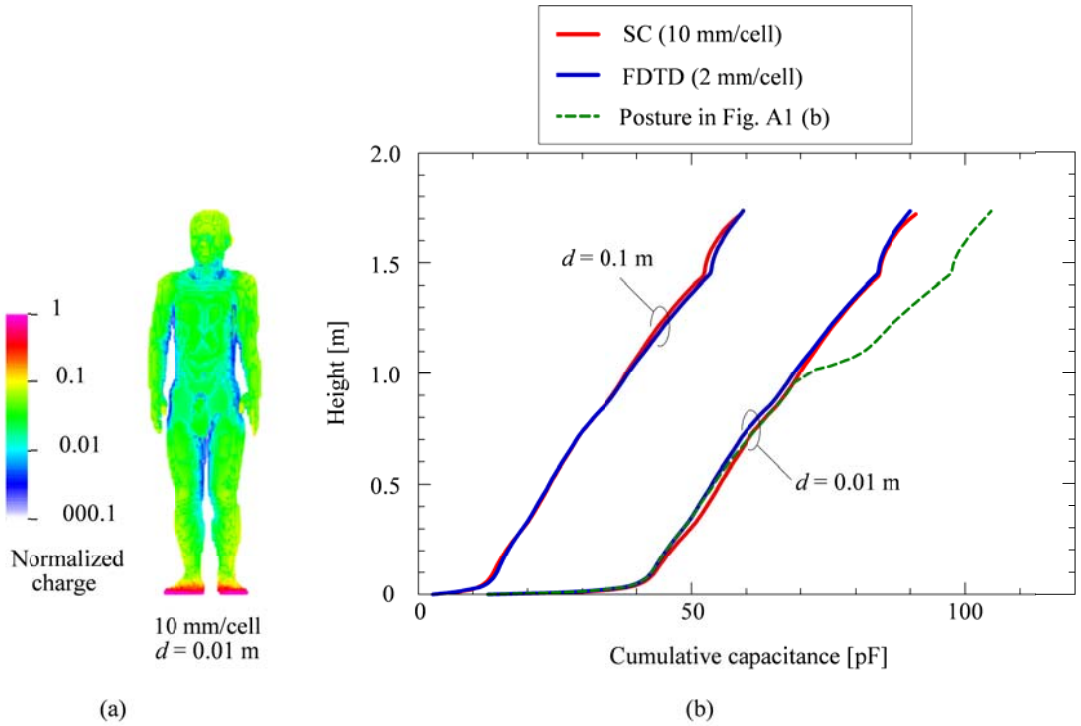

Fig. A3(b)

Table A1

	Human Body Capacitance [pF]	
	Upright	Posture in Fig. 1
Adult male	91	105
Adult female	78	100
3-year-old child	41	56